



**HAL**  
open science

# Iron-Doped CaTiO<sub>3</sub> and Pd/YSZ Dual Bed Catalytic System for CH<sub>4</sub> Emission Control from Natural Gas Vehicle

Maxime Delporte, Helena Kaper, Fabien Can, Nicolas Bion, Xavier Courtois

► **To cite this version:**

Maxime Delporte, Helena Kaper, Fabien Can, Nicolas Bion, Xavier Courtois. Iron-Doped CaTiO<sub>3</sub> and Pd/YSZ Dual Bed Catalytic System for CH<sub>4</sub> Emission Control from Natural Gas Vehicle. *Topics in Catalysis*, 2023, 10.1007/s11244-022-01777-1 . hal-04129440

**HAL Id: hal-04129440**

**<https://hal.science/hal-04129440>**

Submitted on 26 Oct 2023

**HAL** is a multi-disciplinary open access archive for the deposit and dissemination of scientific research documents, whether they are published or not. The documents may come from teaching and research institutions in France or abroad, or from public or private research centers.

L'archive ouverte pluridisciplinaire **HAL**, est destinée au dépôt et à la diffusion de documents scientifiques de niveau recherche, publiés ou non, émanant des établissements d'enseignement et de recherche français ou étrangers, des laboratoires publics ou privés.

## Iron-doped CaTiO<sub>3</sub> and Pd/YSZ dual bed catalytic system for CH<sub>4</sub> emission control from Natural Gas Vehicle.

Maxime Delporte<sup>1,2</sup>, Helena Kaper<sup>2</sup>, Fabien Can<sup>1\*</sup>, Nicolas Bion<sup>1</sup>, Xavier Courtois<sup>1\*</sup>

*1. Institut de Chimie des Milieux et Matériaux de Poitiers (IC2MP), University of Poitiers, CNRS UMR 7285, TSA51106 – F86073 Poitiers Cedex 9, France.*

*2. Laboratoire de Synthèse et Fonctionnalisation des Céramiques, UMR 3080, CNRS/Saint-Gobain CREE, Saint-Gobain Research Provence, 550 Avenue Alphonse Jauffret, Cavaillon, France*

\*corresponding author : [fabien.can@univ-poitiers.fr](mailto:fabien.can@univ-poitiers.fr) (ORCID: 0000-0002-8497-7796); [xavier.courtois@univ-poitiers.fr](mailto:xavier.courtois@univ-poitiers.fr) (ORCID: 0000-0002-0384-1214)

### Abstract

The catalytic treatment of residual traces of refractory methane in the exhaust gas from NGV engines involves the use of expensive, highly loaded precious metal based catalysts. Recently, it was demonstrated that the association of a perovskite with a Pd/YSZ (Yttria-Stabilized Zirconia) catalyst improved both the oxygen exchange behavior on the YSZ support together with the methane oxidation on palladium. However, these interesting results were obtained in condition quite far from an exhaust pipe and this work aims to investigate the concept of this dual catalytic bed system in more realistic conditions. In this study, a mixed electronic/ionic conducting perovskite (CaTi<sub>0.7</sub>Fe<sub>0.3</sub>O<sub>3-δ</sub>) was associated to a pure oxygen ion conductor (YSZ) impregnated with 1% palladium. This dual-bed configuration promoted CH<sub>4</sub> abatement in lean mixture, probably associated to the Pd/PdO active phase formation, but inhibiting effect of both CO<sub>2</sub> and H<sub>2</sub>O was also observed.

**Keywords:** Methane, NGV, Palladium, YSZ, dual-bed

### 1. Introduction

To address the growing energy dependence on traditional fossil fuels and the environmental concerns, the use of natural (bio)gas, which mainly contains methane (90 %), becomes attractive. Pending the development of other clean energy sources, methane has a high energy efficiency that, associated with lower carbon dioxide emissions than other hydrocarbon fuels, offers a viable alternative for combustion engines. Moreover, locally produced bio-gas also induce lower greenhouse gas emission. Interestingly, engines powered by natural gas (NGVs) also produce lower NO<sub>x</sub> and particulate matter emissions than diesel or gasoline engines [1]. Compressed or liquefied natural gas also powers 23 million vehicles worldwide with an annual increase of 20 %, from heavy-duty buses and trucks to light-duty passenger cars [2]. However, the relevance of this option resides in the abatement of unburnt methane in the exhaust gas because of its global warming potential 23 times higher than CO<sub>2</sub>. Hence, the removal of residual traces of refractory methane in the exhaust stream remains a technological challenge which currently implies the use of expensive active materials, which lowers the cost-effectiveness of such alternative systems. Concerning the lean-burn NGVs powered engines, the temperature of the exhaust gas is generally below 500-550 °C [3] and CH<sub>4</sub> oxidation post-treatment should occur in the 320-420 °C temperature range [4] for automotive application. This condition makes the activation of the C-H bond of methane challenging due to its high stability (bond energy: 450 kJ/mol). Among the many catalytic formulations investigated (metal oxide, spinel, perovskite...), platinum-group metals (PGM), are predominant and Pd-containing catalysts have been recognized to be the most active candidate [5]. Still, substantial research efforts for low temperature efficiency must be achieved. Numerous studies were

therefore devoted to the determination of the active phase of the supported palladium materials, depending on the working temperature. The nature of the active sites of Pd catalysts for methane oxidation has been a matter of debate for a long time. It is now recognized that  $\text{PdO} \leftrightarrow \text{Pd}$  phase transformations interplay in the methane oxidation activity. Richard *et al.* [6] reported that the active species of palladium is rather an oxidized state, but the precise nature of the active sites is still controversy since it remains conflicting evidence on the activity of different oxidation states of Pd. For instance, it has been reported that methane is activated on a site pair consisting of an oxygen atom and an oxygen vacancy on the  $\text{PdO}_x$  surface, suggesting a redox mechanism [7,8] where surface oxygen on the palladium crystallites is more active for methane oxidation than bulk oxide due to the higher ability of the oxygen sorption processes [9]. Methane interacts with oxygen on the PdO surface which is rapidly restored by diffusion of bulk oxygen to the surface. This proposed mechanism avoids the need for the coexistence of a separate Pd metal phase in atomic contact with  $\text{PdO}_x$  for methane oxidation. To the opposite, methane oxidation over the metallic Pd surface is controlled by competitive adsorption of methane and oxygen. Overall, PdO catalyzes  $\text{CH}_4$  oxidation via a redox Mars and van Krevelen (MvK) mechanism (with C-H bond activation as the rate-determining step), while metallic Pd catalyzes the reaction via the Langmuir-Hinshelwood mechanism. The nature of catalyst structure in respect to palladium is also discussed in the literature as Pd clusters, Pd clusters surface-saturated with chemisorbed oxygen ( $\text{O}^*$ ), and PdO clusters [10]. The development of active materials dedicated to low temperature application for promotive  $\text{CH}_4$  oxidation refers to the necessity of the coexistence of  $\text{Pd}^0$ , Pd in a reduced state ( $\text{PdO}_x$ ), or oxygen vacancies. The synthesis methods are a tool to control the structure-function of Pd-based catalyst.

Recently Richard *et al.* [6,11,12] proposed an innovative approach in which the methane conversion is boosted by the formation of active oxygen species. With this aim, the catalytic bed was made *via* the association of  $\text{LaMnO}_3+0.2_{\text{wt}\%}\text{Pd/YSZ}$  materials. Yttrium-stabilized zirconia (YSZ) presents oxygen vacancies due to the doping of  $\text{ZrO}_2$  with  $\text{Y}^{3+}$  which exhibits a lower valence state than  $\text{Zr}^{4+}$ . In oxidation catalysis, the improved catalytic performance of YSZ has been attributed to this high concentration of oxygen vacancies [13]. The oxygen exchange behaviour of the Pd/YSZ catalyst was dramatically improved in the presence of  $\text{LaMnO}_3$ . Methane conversion measured in the isotopic exchange set-up also showed a significant improvement. It was postulated that  $\text{LaMnO}_3$  perovskite activated the  $\text{O}_2$  molecule as singlet oxygen, which was then transferred to Pd/YSZ and promoted the methane oxidation *via* a MvK mechanism. However, these interesting results were obtained in conditions quite far from an exhaust pipe, *i.e.* in a recirculating mode with low pressures of methane and oxygen.

In this work, we studied the viability of the concept using a more common synthetic gas bench. Moreover, in order to improve the oxygen exchange behavior compared to the previously implemented perovskite material ( $\text{LaMnO}_3$ ), a mixed ionic and electronic conducting (MIEC) perovskite was selected for this study. Based on  $\text{CaTiO}_3$  material with partial substitution of iron for titanium [14], the  $\text{CaTi}_{0.7}\text{Fe}_{0.3}\text{O}_{3-\delta}$  formulation was chosen after preliminary tests with various rate of titanium substitution for iron (0 to 40 %). The second implemented catalytic system was  $1_{\text{wt}\%}\text{Pd/YSZ}$ . Several YSZ supports were preliminary evaluated. The YSZ oxide provided by TOSOH (8 mol %  $\text{Y}_2\text{O}_3$ -stabilized  $\text{ZrO}_2$ ) was selected for its perfect stability under the reactional mixtures at  $600^\circ\text{C}$ . In addition to evaluation of the proof of the dual-bed concept in a more realistic setup, the influence of both  $\text{CO}_2$  and  $\text{H}_2\text{O}$  was also examined in this work. Additionally, Pd/YSZ behaviors were compared to usual Pd/ $\text{Al}_2\text{O}_3$  sample to highlight the role of palladium active phase formation.

## 2. Materials and Methods

### 2.1 Catalyst preparation

To perform the synthesis of the perovskite  $\text{CaTi}_{0.7}\text{Fe}_{0.3}\text{O}_{3-\delta}$  (denoted as  $\text{CTF}_{30}$ ), calcium nitrate tetrahydrate (99 %, Sigma Aldrich), titanium (IV) isopropoxide (97 %, Sigma Aldrich), iron (III) nitrate nonahydrate (98 %, Sigma Aldrich), palladium (II) nitrate (40,1 %, Enrico Faggi), citric acid (99,6 %, Sigma Aldrich) and glycerol (99,5 %, Sigma Aldrich) precursors were used as received without further purification.

Based on the Pechini method [15], the perovskite was prepared using an adapted protocol to obtain a well crystallized material with no secondary phase and exhibiting a high specific surface area. Ethylene glycol is usually used as chelating agent because of its ability to form an extended covalent network throughout the solution [16]. Based on internal preliminary results, glycerol was used in this study. The desired stoichiometric amount of titanium (IV) isopropoxide was added to the proper amount of glycerol following a cation/ glycerol molar ratio of 1/15. Because of its viscosity, the solution with glycerol was heated to 80 °C. After 45 min of stirring, citric acid was added to the mixture following a molar ratio of 1/7.5 for cation/acid, heated to 80 °C and covered with a watch glass, and stirred for 1 h 30 to dissolve the acid. Calcium nitrate was then added to the mixture and stirred again for 1 h to dissolve the precursor. Iron (III) nitrate was finally added and stirred again for 1 h. The mixture was then heated to 120 °C for 2 h under stirring to ensure the polycondensation of the product until a viscous gel was obtained. The resulting polymer gel was calcined in air in muffle oven first at 100 °C for 1 h (5 °C/min) and at 600 °C for 6 h (1.6 °C/min). The resulting perovskite was grinded and sieved between 125  $\mu\text{m}$  and 250  $\mu\text{m}$  for the catalytic testing.

YSZ (8 mol %  $\text{Y}_2\text{O}_3$ -stabilized  $\text{ZrO}_2$ ) oxide was provided by TOSOH. YSZ-supported metal catalyst (denoted Pd/YSZ) was prepared by wet impregnation of the appropriate amount of palladium (II) nitrate to obtain 1 wt%. The excess of water was evaporated at 60 °C and the resulting powder was dried at 120 °C overnight before calcination at 600 °C during 6 h (5 °C/min) under air flow (150 mL  $\text{min}^{-1}$ ).

A reference palladium supported alumina catalyst, denoted Pd/ $\text{Al}_2\text{O}_3$ , was also prepared with the same impregnation procedure as for Pd/YSZ sample. The  $\text{Al}_2\text{O}_3$  support was provided by Axens.

### 2.2 Catalyst characterizations

X-ray diffraction analysis were carried out with a Bruker D8 Endeavor using a Bragg-Bentano ( $\theta - \theta$ ) geometry equipped with a  $\text{CuK}_\alpha$  cathode radiation source (40 kV and 40 mA). Diffractogram were qualitatively analysed with EVA software from Bruker and ICDD 2016 database. The crystallites sizes were calculated from the Debye-Scherrer equation. To determine lattice parameters of well crystallised  $\text{CaTi}_{0.7}\text{Fe}_{0.3}\text{O}_{3-\delta}$ , the structure was refined by a full-profile analysis method using Full-Prof software [17] and ICSD data corresponding from  $\text{CTF}_{30}$  (ICSD: 93085).

The nitrogen physisorption was performed at 77 K in a Micromeritics Tristar II 3020 instrument. The sample was outgassed under vacuum at 280 °C for 5 h before measurement. Surface area was calculated using the Brunauer-Emmett-Teller [18] (BET) method and the pore size distribution with the Barrett-Joyner-Halenda [19] (BJH) method with Faas correction applied to Halsey equation.

SEM micrographs were obtained with a JEOL FEG JSM-7900F scanning electron microscope operating between 1 kV and 15 kV (special resolution of 0.7 nm) and equipped with an energy-dispersive X-ray spectroscopy (EDXS)

detector. Transmission Electron Microscopy (TEM) micrographs were recorded on JEOL 2100 instrument (operated at 200 kV with a LaB6 source). EDX spectroscopy was carried out with a Hypernine (Premium) detector (active area: 30 mm<sup>2</sup>).

The palladium dispersion was determined by H<sub>2</sub> chemisorption performed using AutoChem 2920 from Micromeritics and 100 mg of Pd/YSZ. After *in situ* reduction under 10 % H<sub>2</sub> at 300 °C (5 °C min<sup>-1</sup>) for 1 h, the sample was flushed at the same temperature under argon for 3 h. The hydrogen was dosed on the sample at 105 °C to prevent hydride formation. After saturation, the sample was flushed under argon for 10 min and exposed again to hydrogen. The amount of chemisorbed hydrogen was taken as the difference between the two hydrogen exposures and exploited as H/M molar ratio. Dispersion (%) and particle size (nm) were determined based on the statistical cuboctahedron clusters model of Drault *et al.* [20].

Temperature programmed reduction experiments were performed on Pd-containing samples with a Micromeritics Autochem 2920 apparatus. The Sample (50 mg) was placed in a U-shaped quartz reactor. Prior the reduction, the catalyst was *in-situ* calcined at 600 °C for 30 min under O<sub>2</sub> (heating rate: 5 °C min<sup>-1</sup>). After cooling to room temperature under argon, the sample was cooling down to -50 °C (coolant setup from Micromeritics, based on the evaporation of liquid nitrogen). The reduction was carried out under 10 % H<sub>2</sub>/Ar up to 400 °C (rate: 10 °C min<sup>-1</sup>). The reduction was followed by a thermal conductivity detector (TCD). Because this TCD is sensitive to water, a H<sub>2</sub>O trap was added downstream the reactor, allowing the quantification of the H<sub>2</sub> consumption.

The Isotopic Exchange experiments were performed in a home-made closed recycling system set-up connected to a Pfeiffer Vacuum quadrupole mass Spectrometer (QMS 200) to monitor the gas phase composition (with Quadera software). The recycling pump placed in the system removes limitation due to gas-phase diffusion (recirculation rate = 170 cm<sup>3</sup>.s<sup>-1</sup>). Tests were performed on catalyst powder sieved between 125 μm and 250 μm. The sample was placed into a U-shaped quartz reactor with quartz wool above and below the catalyst. The involved sample masse was calculated to get the same initial oxygen concentration inside the reactor for all measurements. The sample was first subjected to pure <sup>16</sup>O<sub>2(g)</sub> at 600 °C (10 °C/min, 1 h) prior cooling to 150 °C for Temperature-Programmed Oxygen Isotopic Exchange (TPOIE). The system was then purged under vacuum for 30 min. Pressure of 58 mbar <sup>18</sup>O<sub>2(g)</sub> (≥ 99 at%, ISOTEC) was introduced in the system and the isotopomer distribution was analysed following the intensities of m/z: 32 (<sup>16</sup>O<sub>2</sub>), 34 (<sup>18</sup>O<sup>16</sup>O) and 36 (<sup>18</sup>O<sub>2</sub>). The m/z values of 28 (N<sub>2</sub>), 44 (C<sup>16</sup>O<sub>2</sub>), 46 (C<sup>18</sup>O<sup>16</sup>) and 48 (C<sup>18</sup>O<sub>2</sub>) were also recorded to ensure the absence of atmosphere entrance into the system or desorption of residual carbonated species at the beginning of the exchange process. TPOIE analysis was performed by varying the temperature from 150 °C to 700 °C. The partial pressures of <sup>16</sup>O<sub>2</sub>, <sup>18</sup>O<sup>16</sup>O and <sup>18</sup>O<sub>2</sub> are calculated by the ratio of corresponding intensities of the m/z values of 32, 34, 36 for <sup>16</sup>O<sub>2</sub>, <sup>18</sup>O<sup>16</sup>O and <sup>18</sup>O<sub>2</sub> isotopes, respectively. The atomic fraction of <sup>18</sup>O in the gas-phase (α<sub>g</sub>) is determined by Eq. 1 [21]:

$$\alpha_g = \frac{P_{36} + \frac{1}{2}P_{34}}{P_{32} + P_{34} + P_{36}} \quad (1)$$

## 2.3 Catalytic tests

The catalytic CH<sub>4</sub> oxidation tests were carried out in a fixed bed set-up. For single catalyst test, 100 mg of the catalyst sieved between 125 μm and 250 μm and 100 mg of SiC were mixed and placed inside a quartz reactor. For catalytic tests with a combination of CTF<sub>30</sub> and Pd/YSZ materials (or Pd/Al<sub>2</sub>O<sub>3</sub> sample), 100 mg of each sample samples were implemented, without SiC. Three configurations involving the association of CTF<sub>30</sub> and Pd/YSZ were evaluated: the "dual-bed" noted CTF<sub>30</sub>+Pd/YSZ was composed of a layer of CTF<sub>30</sub> (upstream) in contact with a layer Pd/YSZ (downstream); the "reverse dual-bed" noted Pd/YSZ+CTF<sub>30</sub> was composed of a layer of Pd/YSZ (upstream) in contact with a layer CTF<sub>30</sub> (downstream); the "mechanical mixture" denoted CTF<sub>30</sub>/Pd/YSZ was obtained by an intimate mixing the two powders. The total flow was kept constant to 20 L h<sup>-1</sup>. Catalytic tests are performed from RT to 600 °C (3° min<sup>-1</sup>), followed by a 30 min step at 600 °C before the cooling step. The compositions of the feed gas and effluent stream were monitored continuously during the temperature ascent and descent using online MKS 2030 Multigas infrared analyzer. Various lean gaseous mixtures were examined according to Table 1 and the activities of the different catalytic systems for methane oxidation were recorded successively, corresponding to three consecutive tests starting with the simplified media and then incrementing by adding first CO<sub>2</sub> and then also H<sub>2</sub>O.

**Table1.** Gas feed composition (20 L h<sup>-1</sup>).

Feed/gases	Simplified media	Simplified media +CO <sub>2</sub>	complex media
CH <sub>4</sub>	1500 ppm	1500 ppm	1500 ppm
O <sub>2</sub>	10 %	10 %	10 %
CO <sub>2</sub>	-	10 %	10 %
H <sub>2</sub> O	-	-	8 %
N <sub>2</sub>	balance	balance	balance

## 3. Results and Discussion

### 3.1 Samples characterization

#### 3.1.1 CTF<sub>30</sub> catalyst

After the synthesis, the ICP elemental analysis showed that the expected compositions in Ca, Ti and Fe were obtained for the CTF<sub>30</sub> sample. Additionally, XRD pattern revealed that the perovskite structure was obtained (Figure 1A). The Rietveld refinement indicated an orthorhombic *Pnma/Pbnm* phase (space group #62), with no secondary phases. The crystallite size was estimated at 30 nm from full width half maximum (FWHM) of the main diffraction peak. The specific surface area after ageing at 600 °C was 33 m<sup>2</sup> g<sup>-1</sup> (Table 2). The macroporosity of the material is evidenced on the SEM micrograph (Figure 1B).

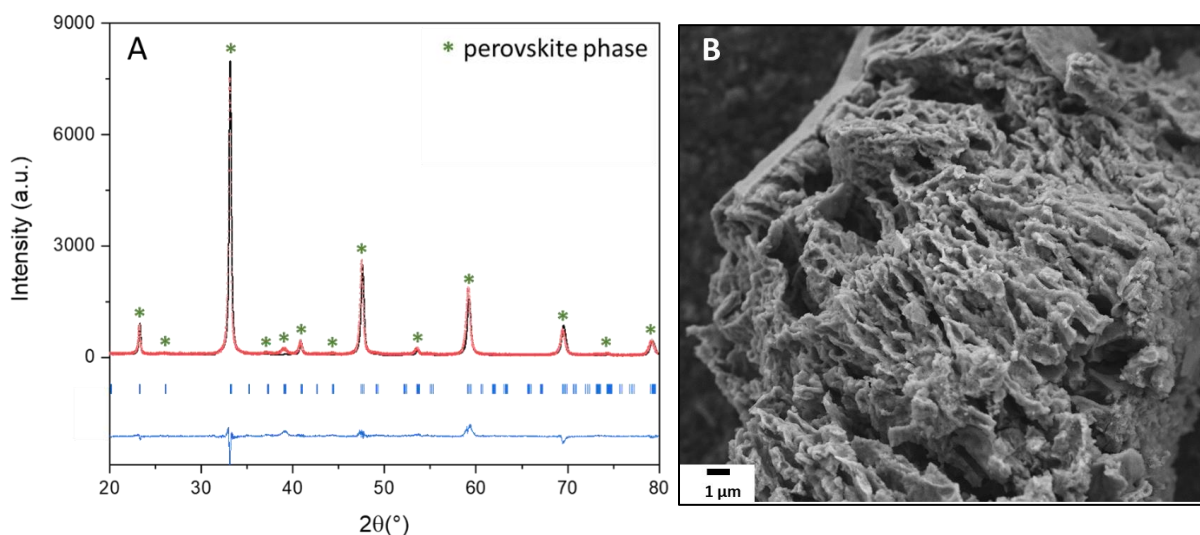


**Figure 1.** (A) XRD pattern of CTF<sub>30</sub> and Rietveld refinement; (B) SEM micrograph.

The partial titanium substitution for iron induces the formation of oxygen vacancies because the ionic radius of 6-coordinated Ti<sup>4+</sup> (0.605 Å) is slightly bigger than for 6-coordinated Fe<sup>4+</sup> (0.585 Å) [22]. Consequently, to maintain the structure and the stoichiometry, most of the iron species are Fe<sup>3+</sup>, with various coordination (Fe<sup>3+</sup> 6-; 5-; 4-coordinated species have ionic radii of 0.645 Å, 0.580 Å and 0.490 Å, respectively, while 6-coordinated Fe<sup>2+</sup> is significantly bigger at 0.780 Å). The characterization by Mössbauer spectroscopy (results not shown) indicated that the Fe<sup>3+</sup> 6-; 5-; 4-coordinated species distribution was 41 %, 46 % and 3 %, respectively, while 10 % Fe<sup>4+</sup> was also detected. The formation of oxygen ion vacancies favours some oxygen exchange behaviour in the solid. This property is studied by isotopic exchange in section 3.1.3.

**Table 2.** Specific surface area, pore volume and size, palladium loading and palladium dispersion of the studied samples.

Samples	Specific surface area (m <sup>2</sup> /g)	Pore volume (cm <sup>3</sup> /g)	Pore size (nm)	Pd loading* (%)	Molar H/M ratio**	D (%)	d (nm)
CTF <sub>30</sub>	33	0.134	14	-	-	-	-
Pd/YSZ	14	0.063	21	1.10	0.64	59	1.8
Pd/Al <sub>2</sub> O <sub>3</sub>	180	0.453	8	1.05	0.51	50	2.2

\* determined by ICP-OES; \*\* M is the total amount of palladium in the sample.

### 3.1.2 Pd/YSZ and Pd/Al<sub>2</sub>O<sub>3</sub> catalysts

Due to the high synthesis temperature for the YSZ support (from TOSOH), the Pd/YSZ catalyst exhibited a low specific surface area, at 14 m<sup>2</sup> g<sup>-1</sup>. On the contrary, Pd/Al<sub>2</sub>O<sub>3</sub> catalysts showed a high specific surface area (180 m<sup>2</sup> g<sup>-1</sup>) which is constant with the support specific surface area, around 200 m<sup>2</sup> g<sup>-1</sup>.

ICP analysis of Pd/YSZ and Pd/Al<sub>2</sub>O<sub>3</sub> samples revealed that the palladium loadings were very close to the expected value of 1 wt% (Table 2). TEM images of the Pd/YSZ catalyst (Figure 2) shows palladium particles located at the borders of the crystallites of the support, allowing precise EDX analysis of the particles. Thus, the observed particles were in the form of PdO oxide. However, a precise count of the particle size distribution was challenging because the observed PdO particles appeared generally highly clustered, with sizes ranging from 5 nm to 10 nm.

However, isolated particles of larger diameter between 10 nm and 20 nm are occasionally observed. The average diameter of the PdO particles from TEM analysis was estimated at 11 nm. In addition, H<sub>2</sub>-chemisorption gives an H/M ratio of 0.64 for the Pd/YSZ catalyst (Table 2). Based on the on the statistical cuboctahedron clusters model of Drault *et al.* [20], the palladium dispersion is estimated at 59 %, which correspond to a mean particle size of 1.8 nm. Compared to the TEM observations, it induces that small particles not identified by microscopy were predominant. The dispersion encountered over Pd/Al<sub>2</sub>O<sub>3</sub> sample is around 50 % (mean particles size: 2.2 nm).

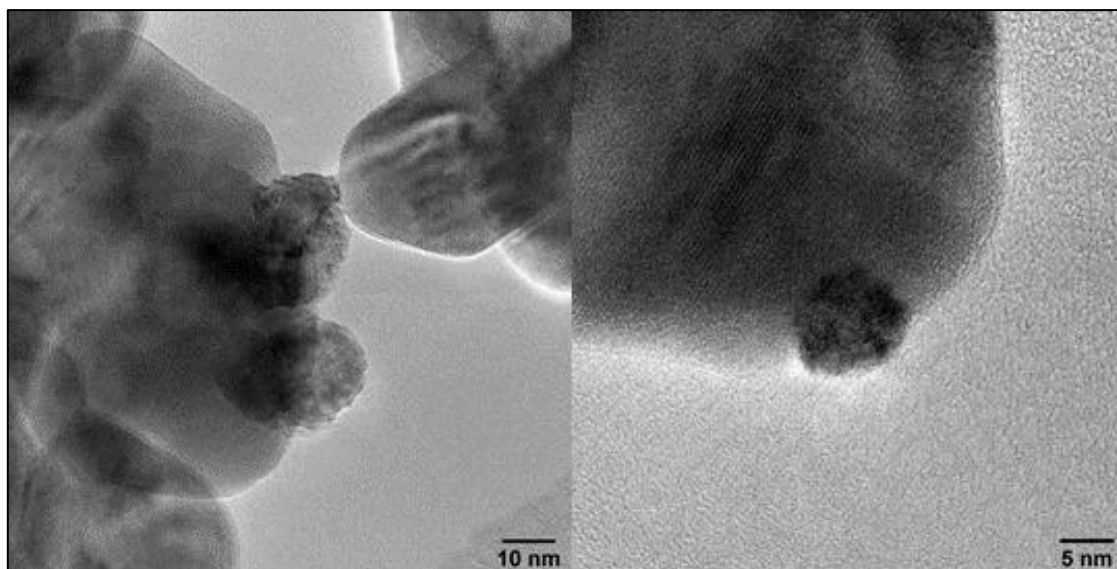


**Figure 2.** TEM images (associated with EDX analysis) at different scales of the Pd/YSZ catalyst.

H<sub>2</sub>-TPR experiments were performed to evaluate the palladium reduction depending on the support, YSZ or Al<sub>2</sub>O<sub>3</sub>. Depending on support formulation, one or two hydrogen consumption peaks can be observed at low temperature [23]. The  $\alpha$  peak is assigned to the reduction of PdO<sub>x</sub> species highly dispersed on the support's surface. The  $\beta$  peak is attributed to stable PdO species having strong interaction with the support. A desorption peak is usually observed near 100 °C. It is related to the decomposition of palladium hydride. Recorded profiles reported Figure 3 shows that the H<sub>2</sub> consumption peak was observed at lower temperature with Pd/Al<sub>2</sub>O<sub>3</sub> (4°C) than with Pd/YSZ (peaks at 32 °C and 77 °C). It results that PdO<sub>x</sub> species supported on Al<sub>2</sub>O<sub>3</sub> are more easily reduced and only one peak of hydrogen consumption was observed. The quantification of the H<sub>2</sub> consumption after subtraction of the H<sub>2</sub> desorption peak confirms that palladium was fully oxidized as PdO species for both samples, in accordance with the TEM-EDX analysis. It also induces that no spillover phenomenon from hydrogen adsorption on the metal to the support is denoted.

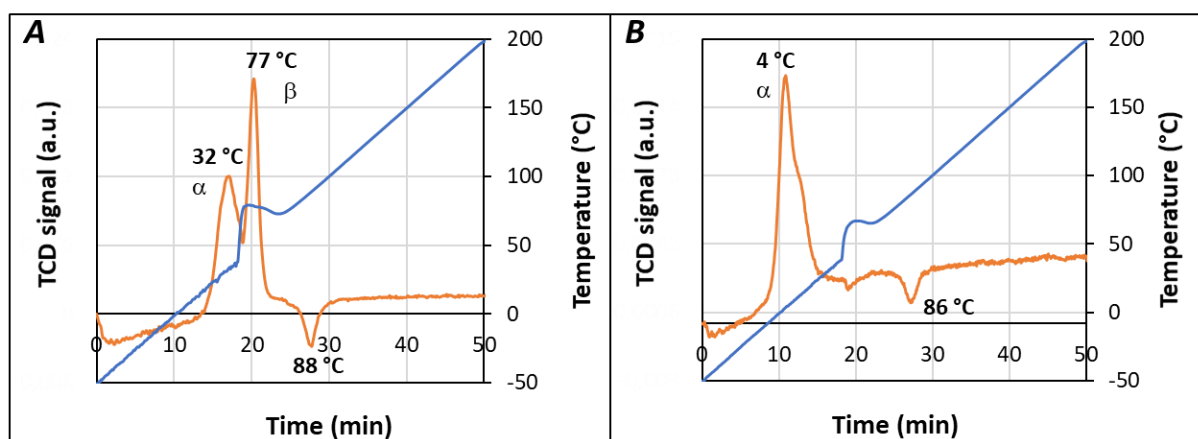


**Figure 3.** TPR profile of Pd/YSZ (A) and Pd/Al<sub>2</sub>O<sub>3</sub> (B). The improperly control of the temperature ramp near 20 min was due to the transition between the cooling and the heating modes.

### 3.1.3 <sup>18</sup>O<sub>2</sub> isotopic exchange

In this section, redox behaviors of the studied catalysts were studied by means of Temperature-Programmed Oxygen Isotopic Exchange (TPOIE). Remind that (i) the setup is made of a recirculating system and (ii) the catalyst masses implemented for the experiments were adjusted to have the same number of oxygen atoms in the solid phase. Consequently, all samples tend to the same equilibrium between the solid phase and the gas phase.

Figure 4A shows the atomic fraction of <sup>18</sup>O in the gas-phase ( $\alpha_g$ ) plotted as a function of temperature obtained with the studied materials. For CTF<sub>30</sub>, the isotopic exchange started at around 270 °C. This temperature is little lower than that previously reported with LaMnO<sub>3</sub> (300 °C) [11], the perovskite which was previously used to highlight the enhancement of O<sub>2</sub> activation on YSZ. The better oxygen exchange behavior of CTF<sub>30</sub> is also illustrated by the temperature recorded to reach 40 % of exchanged atoms in the solid, at 550 °C with LaMnO<sub>3</sub> [11] and 390 °C for CTF<sub>30</sub> (Figure 4A). This result emphasizes the difference in terms of ionic conductivity between LaMnO<sub>3</sub> which is purely electronic conductor and CTF<sub>30</sub> recognized as a MIEC.

Compared to CTF<sub>30</sub>, both Pd/YSZ and Pd/Al<sub>2</sub>O<sub>3</sub> showed a starting exchange temperature shift of 200 °C, at 470 °C (Figure 4A). Palladium-based catalysts are known to be poorly active in isotopic oxygen exchange compared to other noble metal [24]. The exchange equilibrium between the gas phase and the solid ( $\alpha_g$  around 40 %, *i.e.* 60 % of exchanged atoms in the solid) was reached at 650 °C on Pd/YSZ (□). In contrast, due to the poor behavior of Al<sub>2</sub>O<sub>3</sub> support in direct oxygen exchange at low temperatures (T < 500 °C), Pd/Al<sub>2</sub>O<sub>3</sub> (△) did not reach the equilibrium at the end of the test (700 °C). Note that similar exchange onset temperatures were observed on Pd-free YSZ and Al<sub>2</sub>O<sub>3</sub> supports. Consequently, Pd particles do not interfere with the activation of the O<sub>2</sub>-exchange. However, the isotopic distribution was altered since partial pressures of <sup>16</sup>O<sub>2</sub> and <sup>16</sup>O<sup>18</sup>O were detected simultaneously for Pd-supported catalysts, in contrast to Pd-free supports.

The oxygen exchange behavior of the mixed system composed of mechanical mixture of CTF<sub>30</sub> together with Pd/YSZ is also plotted in Figure 4A (◆ symbol). Interestingly, when the CTF<sub>30</sub> is associated to Pd/YSZ, a shift of about 200 °C towards lower temperatures is observed compared to the single-bed Pd/YSZ (□), indicating that the isotopic exchange on Pd/YSZ is significantly improved (half of the exchangeable atoms are provided by YSZ in this test). The promotion of O<sub>2</sub> exchange over YSZ support was previously observed by Richard *et al.* [12] with LaMnO<sub>3</sub> as implemented perovskite. It was proposed that the formation of an active oxygen species on the

perovskite was involved to promote the exchange on YSZ at lower temperatures. The generated active species on the perovskite which promote the oxygen exchange on YSZ remains unclear but the assumption of singlet ( $^1\Delta_g$ ) oxygen formation over  $\text{LaMnO}_3$  was speculated [11]. This highly reactive intermediate ( $^1\Delta_g$ ) $\text{O}_2$  can thereafter enhance the oxygen exchange of YSZ.

Various configurations involving the same weight of  $\text{CTF}_{30}$  and Pd/YSZ, as described in section 2.3, were also evaluated: the "dual-bed" noted  $\text{CTF}_{30}+\text{Pd/YSZ}$ , the "reverse dual-bed" noted  $\text{Pd/YSZ}+\text{CTF}_{30}$  and the "mechanical mixture" denoted  $\text{CTF}_{30}/\text{Pd/YSZ}$ . Note that the total weight of the catalytic bed was adjusted to get the same amount of oxygen atoms inside the reactor for all measurements. Oxygen exchange profiles plotted in Figure 4B are quite similar for all configurations. However, the mechanical mixture showed the best results.

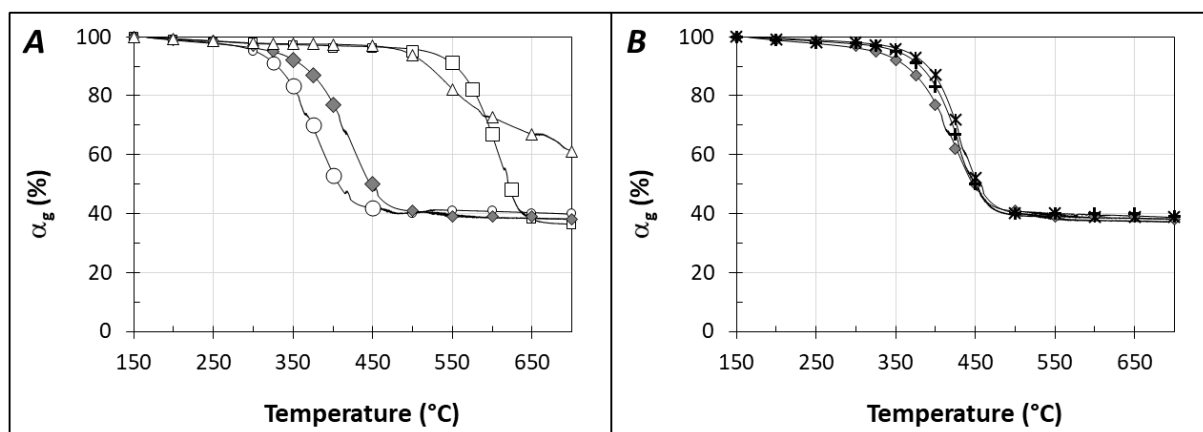


**Figure 4.** Evolution of the atomic fraction of  $^{18}\text{O}$  in the gas-phase ( $\alpha_g$ ) (%) depending on temperature for (A): the comparison of single ( $\text{CTF}_{30}$  (○), Pd/YSZ (□), Pd/Al<sub>2</sub>O<sub>3</sub> (△)) and mixed system ( $\text{CTF}_{30}/\text{Pd/YSZ}$  (◆)).

(B): configurations involving the association of both  $\text{CTF}_{30}$  and Pd/YSZ: dual bed  $\text{CTF}_{30}+\text{Pd/YSZ}$ (+); reverse dual bed  $\text{Pd/YSZ}+\text{CTF}_{30}$  (\*); mechanical mixture  $\text{CTF}_{30}/\text{Pd/YSZ}$ (◆).

### 3.2 Catalytic tests

Note that the CO was never detected whatever the tests reported below, proving the total oxidation reaction of methane.

#### 3.2.1 Single $\text{CTF}_{30}$ and Pd/YSZ catalysts

First, single  $\text{CTF}_{30}$  and Pd/YSZ catalysts were evaluated in simplified media with neither  $\text{CO}_2$  nor  $\text{H}_2\text{O}$ , up to 600 °C, in both temperature rise and descent. Results are presented Figure 5. Note that the catalytic performances of single Pd/Al<sub>2</sub>O<sub>3</sub> sample are discussed in section 3.2.3.

For  $\text{CTF}_{30}$ , the methane conversion started from 350 °C and it increased up 78 % at 600 °C. The conversion rate remained constant during the 30 min step at 600 °C and the profile recorded during temperature descent (dotted line) was similar to the ascent behavior. It appears that  $\text{CTF}_{30}$  remained very stable under reaction flow even after the 600 °C step for 30 min.

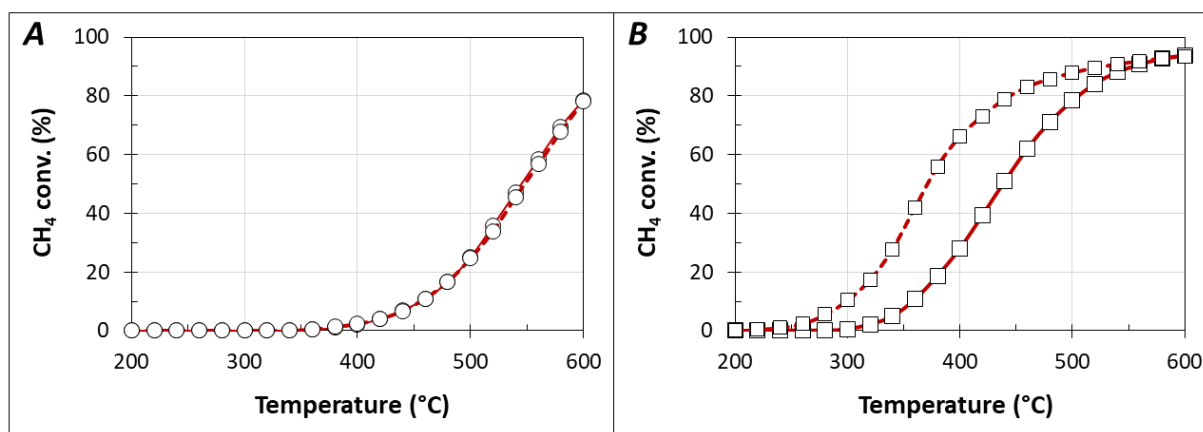


**Figure 5.** Methane conversion recorded during ascent (full line) and descent (dotted line) of temperature in simplified media ( $\text{CH}_4+\text{O}_2$ ; —) for (A):  $\text{CTF}_{30}$  (○) and (B): Pd/YSZ (□).

The YSZ support was not active in methane oxidation (results not shown) but, as expected, the Pd/YSZ catalyst (Figure 5B) was more active than the  $\text{CTF}_{30}$  perovskite, with a start of conversion at 300 °C observed for the ascent test (full line). A conversion of 93 % was reached at 600 °C. To the opposite of  $\text{CTF}_{30}$ , higher performances were denoted during the temperature descent. For instance, the conversion observed at 400 °C was 66 % during the temperature decrease against 28 % during the temperature ascent. The conversion dropped to 0 % at around 225 °C, compared to the start of activation at 300 °C during the run-up test. This enhanced conversion after the 600 °C step can be attributed to a change in the palladium redox state under the reaction mixture. The total methane oxidation tests were performed without any pretreatment after the synthesis calcination step. It is therefore accepted, in agreement with the TEM and TPR analyses, that palladium was initially in the oxide form as PdO. The partial palladium oxide reduction would occur during the first light-off test together with the methane conversion. Indeed, Mahara *et al.* [25] demonstrated by *in situ* EXAFS analysis that the presence of  $\text{CH}_4$  resulted in the partial reduction of the easily reducible surface PdO on the particle surface. At higher temperature under  $\text{CH}_4$  media (600 °C), the decomposition/reduction of PdO was enhanced, generating additional Pd<sup>0</sup> sites [26]. Su *et al.* [27] showed that the reduction of PdO under  $\text{CH}_4$  led to a nucleation of Pd<sup>0</sup> within the PdO particles, unlike the reduction under  $\text{H}_2$  which generated a layer of Pd<sup>0</sup> on the PdO surface. Finally, the highest  $\text{CH}_4$  oxidation performances observed for the temperature descent can be attributed to a complex active Pd<sup>0</sup>/PdO phase formed during the ascent test and the step at 600 °C. In fact, the former generated Pd<sup>0</sup> at 600 °C can be partially re-oxidized for temperature lower than approximately 500 °C, leading to migration and encapsulation of Pd<sup>0</sup>. Then, the highly active species of Pd/YSZ is revealed by a multi-step PdO reduction mechanism involving nucleation, growing and encapsulation. Finally, note that PdO → Pd<sup>0</sup> phase transformations is subject to temperature.

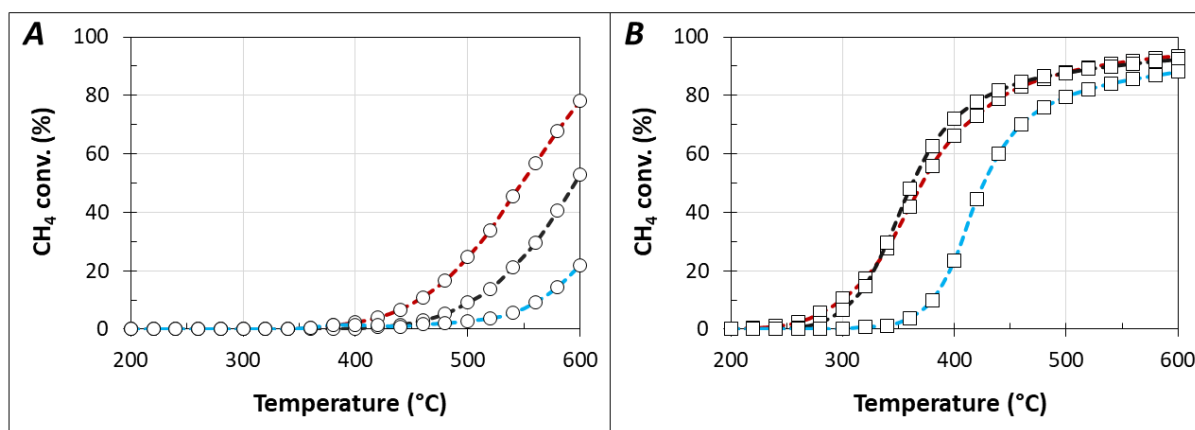


**Figure 6.** Impact of the reaction mixture on methane conversion recorded during descent of temperature: ( $\text{CH}_4+\text{O}_2$ : —); ( $\text{CH}_4+\text{O}_2+\text{CO}_2$ : —); ( $\text{CH}_4+\text{O}_2+\text{CO}_2+\text{H}_2\text{O}$ : —) in for (A): single  $\text{CTF}_{30}$  (○) and (B): single Pd/YSZ (□).

The impact of competing compounds such as  $\text{CO}_2$  and  $\text{H}_2\text{O}$  on the activity of materials in the total oxidation of methane was studied depending on the fed mixtures reported in Table 1. For  $\text{CTF}_{30}$  sample, the conversion profiles were similar for each evaluated reaction mixture for both successive ascent and descent tests, as illustrated in Table 3 which reports the variation in temperature for 20% methane conversion ( $T_{20}$ ). Then,  $\text{CTF}_{30}$  catalyst remained stable whatever the composition of the reaction mixture. Figure 6A compares the conversion profiles recorded during the temperature descent. The addition of  $\text{CO}_2$  in the reaction mixture led to a general decrease in  $\text{CH}_4$  conversion over  $\text{CTF}_{30}$ . Indeed, the conversion started 50 °C higher compared with the simplified mixture and reached a maximum of 54 % at 600°C. Considering the high stability of the perovskite, the loss of conversion observed in Figure 6A can be directly associated only to the presence of carbon dioxide and not to deactivation due to the succession of catalytic tests. The basicity of calcium coupled with the acidic properties of carbon dioxide should induce the formation of carbonate species on the surface of  $\text{CTF}_{30}$ , thus limiting the adsorption and dissociation of methane on the active iron sites close to calcium. This assumption is supported by the fact that active sites for methane conversion on CTF samples are related to iron environment [28]. The catalytic test in the presence of  $\text{H}_2\text{O}$  in addition to  $\text{CO}_2$  showed a further decrease in methane conversion. The onset was then observed at 475 °C and the conversion reached a maximum of only 21 % at 600 °C. The deactivation of catalysts in the presence of water has been widely observed by many authors on metal catalysts [29]. The addition of  $\text{H}_2\text{O}$  would lead to the formation of OH groups on the catalyst surface, preventing the oxidation reaction of methane on the active iron sites. Additional catalytic tests were performed in the presence of  $\text{H}_2\text{O}$  but without  $\text{CO}_2$  and the resulting conversions (not shown) were similar than that observed in full complex media ( $\text{CH}_4+\text{O}_2+\text{CO}_2+\text{H}_2\text{O}$ , blue curve Figure 6A). Water is then mainly responsible for the inhibition of the activity when all gases are fed in the reaction mixture.

**Table 3.** Temperature for 20 % of  $\text{CH}_4$  conversion ( $T_{20}$ ) depending on the inlet gas mixture.

sample	$\text{CTF}_{30}$			Pd/YSZ		
	Ascent test	Descent test	$\Delta$ (descent-ascent)	Ascent test	Descent test	$\Delta$ (descent-ascent)
$\text{CH}_4+\text{O}_2$	488 °C	488 °C	0°C	382 °C	326 °C	-56°C
$\text{CH}_4+\text{O}_2+\text{CO}_2$	534 °C	537 °C	+3°C	340 °C	328 °C	-12°C
$\text{CH}_4+\text{O}_2+\text{CO}_2+\text{H}_2\text{O}$	596 °C	595 °C	-1°C	410 °C	396 °C	-14°C

Concerning single Pd/YSZ catalyst, the presence of CO<sub>2</sub> and H<sub>2</sub>O had different impacts than those observed on CTF<sub>30</sub>. Indeed, the methane conversion recorded during the temperature descent reaction in the presence of CO<sub>2</sub> globally followed the profile recorded with the simplified mixture (Figure 6B). However, the methane conversion returned to 0 % at around 225 °C in simplified media, while it started near 260°C in the successive test with addition of CO<sub>2</sub> in the reactional mixture (curve not shown). T<sub>20</sub> temperatures reported in Table 3 also illustrate the inhibiting effect of CO<sub>2</sub> on Pd/YSZ at low temperature (326°C in descant test in simplified mixture *vs.* 340°C for the successive ascent test in presence of CO<sub>2</sub>). Note that the CO<sub>2</sub> poisoning effect appeared reversible since conversions curves were superposed from 550°C for ascent and descent tests. Moreover, data reported in Table 3 also illustrates that the palladium activation still occurred in presence of CO<sub>2</sub>, but in a lower extent than that observed in simplified media, with a decrease of 12°C in T<sub>20</sub> between the ascent and descant test in presence of CO<sub>2</sub>. Then, the palladium active phase was mainly generated under CH<sub>4</sub> during the first test proceeded in simplified condition.

Under wet media (CH<sub>4</sub>+O<sub>2</sub>+CO<sub>2</sub>+H<sub>2</sub>O), the methane conversion was strongly inhibited. It started near 340°C, *i.e.* at a much higher temperature compared to the previous inlet mixtures. Despite an improvement observed during the descent test, a shift of the methane conversion curve of approximately 70 °C to higher temperature was observed compared to tests performed without H<sub>2</sub>O (Figure 6B, Table 3). Compared to the first run under simplified media (Figure 5B, full line), the recorded conversion in temperature cooling under wet media was lower in the 300-400 °C temperature range (until 8 conversion points at 380 °C) and a little higher in the 400-500 °C temperature range (maximum gap: 8 conversion points at 440 °C). This inhibiting effect of water is largely reported in the literature. For low temperature application (T<400 °C), both the recombination of surface hydroxyl and water desorption from the catalyst control reactivity of methane oxidation over PdO, making the water desorption from the surface the rate-limiting step for methane oxidation [30]. Therefore, the poisoning effect of water was proposed to be due to the formation of palladium (II) hydroxide where the breaking of the OH bond in the hydroxide is the determining-step [31]. At higher temperature, (T>400 °C), OH groups tend to desorb and the inhibiting effect of H<sub>2</sub>O is attenuated.

The influence of CO<sub>2</sub> and H<sub>2</sub>O on the structure-function relationship of Pd/YSZ catalyst was further investigated by recording the conversion of methane at 350 °C under different reaction mixtures. Results reported Figure 7 obviously confirms the previous statements. Under simplified media (CH<sub>4</sub>+O<sub>2</sub>), methane conversion increased during time on stream, associated to the continuous formation of the more active Pd<sup>0</sup>/PdO phase. CH<sub>4</sub> conversion started at 11 % to reach 20 % after 80 minutes due to PdO reduction by methane. With the addition of CO<sub>2</sub> to the reaction flow, the CH<sub>4</sub> conversion first dropped to 12 % and then increased continuously to 28 % after 90 minutes. This confirms that CO<sub>2</sub> does not limit the generation of the active phase of the catalyst but alters their accessibility. Finally, as expected, H<sub>2</sub>O addition revealed a drastic decline in methane conversion confirming that carbon dioxide has a lower poisoning effect than water [32]. Note that the influence of water on the catalyst activity is reported to be sensitive to the type of host materials. Supports with high oxygen mobility show potential to moderate the inhibition by water, accelerating hydroxyl desorption [33].

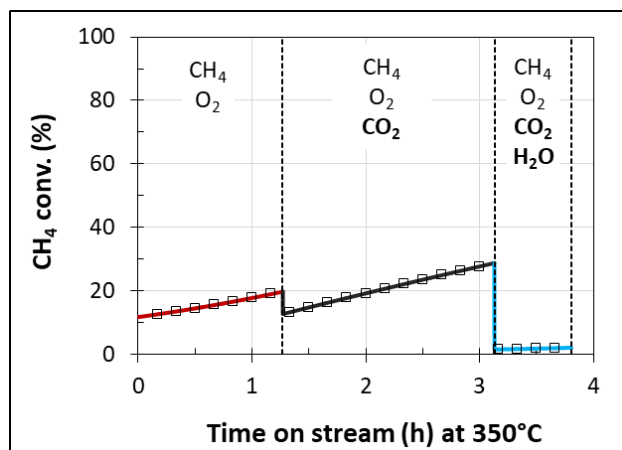


**Figure 7.** Pd/YSZ ( $\square$ ) methane conversion at 350°C depending on the time on stream under various gaseous media ( $\text{CH}_4+\text{O}_2$ : —;  $\text{CH}_4+\text{O}_2+\text{CO}_2$ : —;  $\text{CH}_4+\text{O}_2+\text{CO}_2+\text{H}_2\text{O}$ : —)

### 3.2.2 Dual $\text{CTF}_{30}$ and Pd/YSZ system

As described in section 2.3, three configurations in the Pd/YSZ- $\text{CTF}_{30}$  association were studied, namely the dual-bed ( $\text{CTF}_{30}+\text{Pd/YSZ}$ ), the reverse dual-bed Pd/YSZ+ $\text{CTF}_{30}$ ) and the mechanical mixture ( $\text{CTF}_{30}-\text{Pd/YSZ}$ ). These configurations should highlight the specific function of  $\text{CTF}_{30}$  toward Pd/YSZ. As mentioned in the introduction part, it was postulated that perovskite material can activate the  $\text{O}_2$  molecule which can be used on Pd/YSZ *via* the oxygen mobility of the YSZ support, to promote the methane abatement. However, this assumption required confirmation in a more realistic catalytic setup.

First, the influence of the catalytic bed configuration was examined. The methane conversion recorded in simplified media during the temperature decrease is reported Figure 8A. The reversed bed configuration showed the lowest activity. Interestingly, the methane conversion was then similar to that recorded with the single Pd/YSZ sample (Figure 6B). This result can be explained by the facts that (i)  $\text{CTF}_{30}$  showed no activity at temperature lower than 400 °C and (ii) the postulated active species generated over  $\text{CTF}_{30}$  should not interact with Pd/YSZ placed upstream. On the contrary, a significant improvement was obtained with the mechanical mixture, which highlights the importance of the amount of contact points between  $\text{CTF}_{30}$  and Pd/YSZ in the activity improvement. The beneficial effect of the  $\text{CTF}_{30}+\text{Pd/YSZ}$  mechanical mixture was also evidenced during the isotopic exchange experiments (Figure 4B), but in a lower extent which can be attributed to the recirculating mode used for TPOIE experiments.

A focus on the methane conversion obtained at 400 °C is depicted Figure 8B to compare single and the mixed catalytic system. While  $\text{CTF}_{30}$  alone was nearly inactive at 400 °C (2 % conversion), the association with Pd/YSZ led to an exaltation of the activity, with 62 %  $\text{CH}_4$  conversion against only 29 % for single Pd/YSZ in the ascent test. It is then clearly evidenced that mechanical mixture of  $\text{CTF}_{30}$  and Pd/YSZ ( $\blacklozenge$ ) allowed higher  $\text{CH}_4$  conversion in simplified media ( $\text{CH}_4+\text{O}_2$ ) than the added contribution of each catalyst. The observed phenomenon was not cumulative but synergetic. Similar benefits were also observed during the descent tests reported, with 87 % methane conversion at 400 °C with the mechanical mixture  $\text{CTF}_{30}-\text{Pd/YSZ}$ , compared to 66 % and 2 % for single Pd/YSZ and  $\text{CTF}_{30}$ , respectively. Thus, the concept of a beneficial effect of  $\text{CTF}_{30}$  toward Pd/YSZ for  $\text{CH}_4$  abatement in simplified media is clearly evidenced.

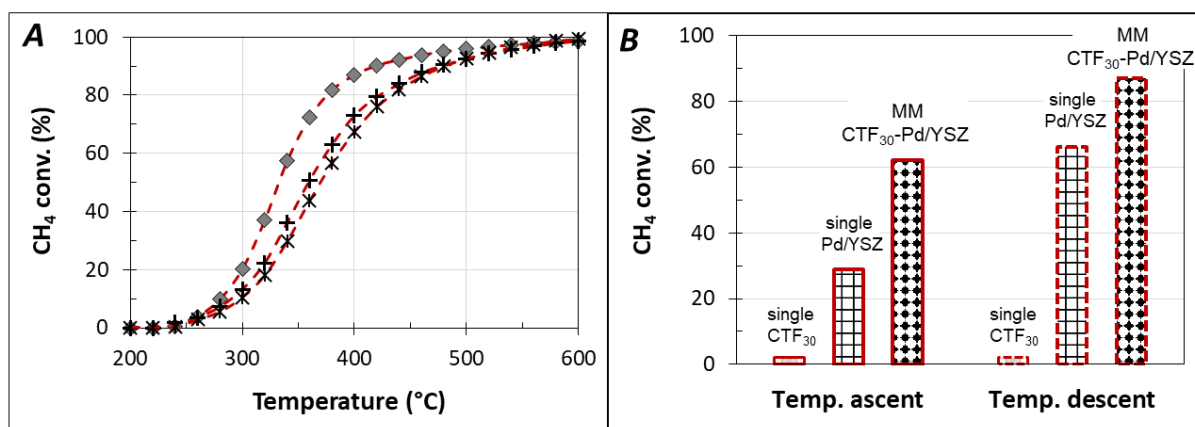


**Figure 8.** (A): Impact of catalytic bed configuration on the CH<sub>4</sub> conversion recorded during the descent of temperature in simplified mixture (CH<sub>4</sub>+O<sub>2</sub>): dual bed CTF<sub>30</sub>+Pd/YSZ(+); reverse dual bed Pd/YSZ+CTF<sub>30</sub> (\*); mechanical mixture CTF<sub>30</sub>/Pd/YSZ(◆).

(B): CH<sub>4</sub> conversion at 400 °C recorded in simplified mixture during the ascent/descent temperature for single CTF<sub>30</sub> (○), Pd/YSZ (□) and the mechanically mixture CTF<sub>30</sub>-Pd/YSZ (◆) catalytic bed.

The influence of the reactional mixture composition was then investigated with the mechanical mixed bed configuration (CTF<sub>30</sub>-Pd/YSZ). Only the results recorded during the descent tests are discussed in this section. Figure 9A shows that CO<sub>2</sub> addition shifted the CH<sub>4</sub> conversion curve toward higher temperatures, while results depicted in section 3.2.1 previously showed that for single catalysts, only CTF<sub>30</sub> was significantly CO<sub>2</sub> sensitive. For Pd/YSZ, the CO<sub>2</sub> inhibiting effect was compensated by the palladium activation occurring during the tests (Figure 6B). Consequently, the decrease in methane conversion recorded with the CTF<sub>30</sub>-Pd/YSZ mechanical mixture with CO<sub>2</sub> in the feed stream is mainly attributable to the CTF<sub>30</sub> sample. Moreover, compared to the synergetic effect obtained using the simplified reactional mixture (Figure 9B), the gain in methane conversion was significantly attenuated by CO<sub>2</sub> (Figure 9C). Only a small improvement was still observed. Then, the availability of activated oxygen species responsible for methane conversion improvement became very limited. Since CTF<sub>30</sub> exhibited basic calcium sites, the formation of surface carbonates species is assumed. Carbonates species are well-known to favor oxygen exchange reactions [34]. The generated active oxygen species was postulated to be a singlet O<sub>2</sub>. The exchange between the active oxygen species and the surface carbonates could explain the singlet O<sub>2</sub> relaxation, leading to the decrease in the availability of this species.

Figure 9A also shows that the water inhibition effect appeared more significant than the CO<sub>2</sub> one, in accordance with the results previously discussed for single CTF<sub>30</sub> and Pd/YSZ catalysts (Figure 6). The gain in methane conversion with the CTF<sub>30</sub>-Pd/YSZ association was then negligible (Figure 9C). The improvement observed for temperatures higher than 500 °C is attributable to the contribution of the CTF<sub>30</sub> sample but no synergetic effect was then observed.

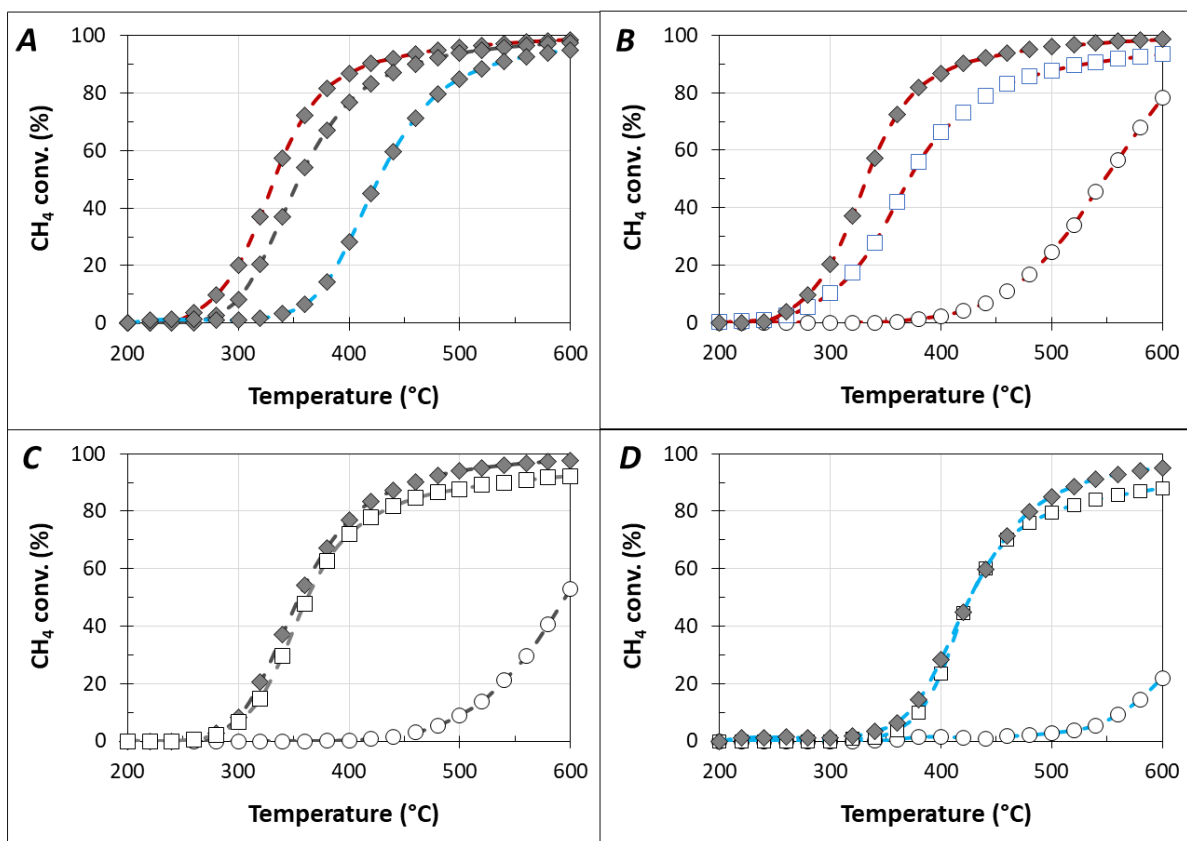


**Figure 9.** (A): Influence of the gaseous media composition ( $\text{CH}_4+\text{O}_2$ : —;  $\text{CH}_4+\text{O}_2+\text{CO}_2$ : —;  $\text{CH}_4+\text{O}_2+\text{CO}_2+\text{H}_2\text{O}$ : —) on the methane conversion obtained with the Mechanically Mixture catalytic bed  $\text{CTF}_{30}\text{-Pd/YSZ}$ , recorded during the descent of temperature.

(B):  $\text{CH}_4$  conversion under  $\text{CH}_4+\text{O}_2$  (—) reactional mixture recorded during the descent of temperature for single  $\text{CTF}_{30}$  (○),  $\text{Pd/YSZ}$  (□) and the Mechanically Mixture  $\text{CTF}_{30}\text{-Pd/YSZ}$  (◆).

(C):  $\text{CH}_4$  conversion under  $\text{CH}_4+\text{O}_2+\text{CO}_2$  (—) reactional mixture recorded during the descent of temperature for single  $\text{CTF}_{30}$  (○),  $\text{Pd/YSZ}$  (□) and the mechanically mixture  $\text{CTF}_{30}\text{-Pd/YSZ}$  (◆).

(D):  $\text{CH}_4$  conversion under  $\text{CH}_4+\text{O}_2+\text{CO}_2+\text{H}_2\text{O}$  (—) reactional mixture recorded during the descent of temperature for single  $\text{CTF}_{30}$  (○),  $\text{Pd/YSZ}$  (□) and the mechanically mixture  $\text{CTF}_{30}\text{-Pd/YSZ}$  (◆).

### 3.2.3 Mechanistic aspect- Role of the perovskite

In addition to the role of the  $\text{CTF}_{30}$  perovskite, catalytic tests revealed an activation of the palladium phase in  $\text{Pd/YSZ}$ . Based on the bibliography [25,26,27], it is assumed that  $\text{PdO} \rightarrow \text{Pd}^0$  phase transformation initiated under the reactional mixture interplayed in the oxidation of methane. To date, the identification of the optimum palladium phase at temperature lower than  $600\text{ }^\circ\text{C}$  and the details of the mechanism remain a much-debated topic.  $\text{PdO}$  is generally admitted to be the more active phase at high temperature ( $T \geq 600\text{ }^\circ\text{C}$ ), while substantial evidences suggest the necessity of the coexistence of  $\text{Pd}^0$ ,  $\text{PdO}_x$  (Pd in a reduced state), or even oxygen vacancies ( $V_{\text{O}}$ ). In this work, the association of  $\text{CTF}_{30}$  with  $\text{Pd/YSZ}$  led to a significant  $\text{CH}_4$  conversion enhancement in simplified reactional mixture, mainly for the mechanical mixing configuration with intimate contacts. As previously observed in [11], it is associated with the promotion of the  $\text{O}_2$  exchange on  $\text{Pd/YSZ}$ , which was supposed to assist the methane oxidation reaction through a MvK mechanism. Interestingly, the conversion curve recorded using the simplified gas mixture ( $\text{CH}_4+\text{O}_2$ ) with the  $\text{CTF}_{30}\text{-Pd/YSZ}$  mechanical mixture during the first ascent (first test, profile not shown) was very similar to that obtained for the descent with single  $\text{Pd/YSZ}$  catalyst (after palladium activation, Figure 5B). It could induce that the beneficial effect of  $\text{CTF}_{30}$  also interfered with the palladium state. In fact,

palladium state and methane activation are linked since PdO reduction is assumed to occur together with methane oxidation, assuming that PdO was the initial palladium state as evidenced by the TPR measurements.

To highlight the role of CTF<sub>30</sub> material in the enhancement of the catalytic activity, the association with Pd/Al<sub>2</sub>O<sub>3</sub> was also examined. This sample was selected because it is a reference catalyst for this application and because alumina showed poor oxygen exchange properties, as described in Figure 4A. The palladium particle size determined by H<sub>2</sub>-chemisorption was around 2.2 nm for Pd/Al<sub>2</sub>O<sub>3</sub> catalyst, compared to 1.8 nm for Pd/YSZ (Table 2). This similar particle size close to 2 nm allows to rule out the possible structure sensitivity of the reaction. Single Pd/Al<sub>2</sub>O<sub>3</sub> catalyst was evaluated in simplified CH<sub>4</sub>+O<sub>2</sub> media and compared to Pd/YSZ Figure 10A. The methane conversion recorded during the first ascent test with Pd/Al<sub>2</sub>O<sub>3</sub> ( $\Delta$ , full line) was significantly higher than that observed with Pd/YSZ ( $\square$ , full line). Again, the methane conversion recorded during the temperature descent with Pd/Al<sub>2</sub>O<sub>3</sub> was higher compared with the ascent test ( $\Delta$ , dotted line), as previously evidenced for Pd/YSZ sample, indicating the formation of a more active palladium phase. Figure 10B compares the methane conversion recorded at 400 °C in simplified mixture depending on the catalytic system. Interestingly, the mechanical mixture CTF<sub>30</sub>-Pd/Al<sub>2</sub>O<sub>3</sub> allowed the same conversion during the first ascent experiment than single Pd/Al<sub>2</sub>O<sub>3</sub> in descent test (observed on the whole temperature range). Then, the presence of CTF<sub>30</sub> was also beneficial for the formation of the more active palladium phase on Pd/Al<sub>2</sub>O<sub>3</sub>. Unfortunately, it did not provide a supplementary enhancement of the methane conversion after the PdO/Pd<sup>0</sup> active phase formation. Both Pd/YSZ and Pd/Al<sub>2</sub>O<sub>3</sub> catalysts exhibited PdO as initial palladium state. However, the TPR experiments showed that PdO on Al<sub>2</sub>O<sub>3</sub> is more easily reducible than on YSZ. This result is consistent with the assumption that the PdO/Pd<sup>0</sup> active phase formation occurred more rapidly on Pd/Al<sub>2</sub>O<sub>3</sub> than on Pd/YSZ. Then, it is assumed that in CTF<sub>30</sub>-Pd/YSZ association, active O<sub>2</sub> generation helped the methane conversion concomitantly with PdO partial reduction.

Figure 10B also shows that both single Pd/Al<sub>2</sub>O<sub>3</sub> and mechanical mixture CTF<sub>30</sub>-Pd/Al<sub>2</sub>O<sub>3</sub> showed similar conversion during the descent test. It seems to indicate that the decisive step remains the generation of a Pd<sup>0</sup>/PdO<sub>x</sub> phase, irrespective of the support properties. Nevertheless, the decomposition and reformation of Pd-based active phase for methane oxidation is strongly dependent on the nature of the support [26]. Over Pd/YSZ, mechanisms for the low temperature combustion of methane include steps for oxygen exchange between the palladium phase and the support [35]. As a consequence, it is postulated that PdO/Pd<sup>0</sup> reciprocation on the Pd/YSZ catalyst is assisted by the synergetic effect of CTF<sub>30</sub> material. As previously discussed, the assumption of active ( $\Delta_g$ )O<sub>2</sub> formation by CTF<sub>30</sub> enhances the oxygen transfer ability of YSZ involved in the methane conversion. It is then tentatively assumed that YSZ offers oxygen exchange to tune the valence state of palladium species by the redistribution of active palladium phase [36].

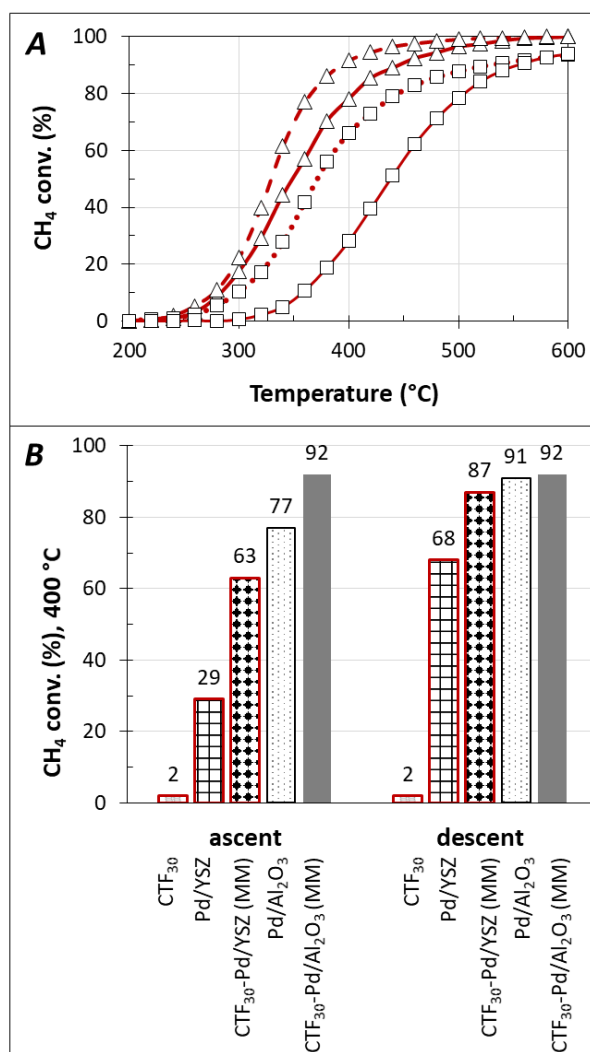


**Figure 10.** (A): Methane conversion recorded during ascent (full line) and descent (dotted line) of temperature in simplified media (CH<sub>4</sub>+O<sub>2</sub>: —) with single Pd/YSZ (□) and single Pd/Al<sub>2</sub>O<sub>3</sub> (△);

(B): Methane conversion recorded at 400°C in simplified media (CH<sub>4</sub>+O<sub>2</sub>) during ascent and descent tests depending on the catalytic system: single CTF<sub>30</sub>; single Pd/YSZ; CTF<sub>30</sub>-Pd/YSZ mechanical mixture; single Pd/Al<sub>2</sub>O<sub>3</sub>; CTF<sub>30</sub>-Pd/Al<sub>2</sub>O<sub>3</sub> mechanical mixture.

#### 4. Conclusions

For the first time, the beneficial association of a perovskite with palladium-based catalysts for the total methane oxidation was confirmed using a synthetic gas bench setup dedicated to catalytic tests. The observed synergetic effect observed in simplified gas mixture was associated to the formation of active oxygen species on the perovskite, which were then transferred to the palladium-based catalyst allowing the promotion of the methane oxidation. This synergetic effect is favored by intimate contacts between CaTi<sub>0.7</sub>Fe<sub>0.3</sub>O<sub>3-δ</sub> and Pd/YSZ, obtained by a mechanical mixture. The promoting effect of CaTi<sub>0.7</sub>Fe<sub>0.3</sub>O<sub>3-δ</sub> perovskite is partially inhibited by the presence of 10 % CO<sub>2</sub> in the reactional mixture, and fully inhibited with the supplementary 8 % H<sub>2</sub>O. Comparison with the association of the CaTi<sub>0.7</sub>Fe<sub>0.3</sub>O<sub>3-δ</sub> perovskite with a Pd/Al<sub>2</sub>O<sub>3</sub> catalyst indicates that the decisive step of the methane oxidation remains the generation of a Pd<sup>0</sup>/PdO<sub>x</sub> phase, irrespective to the support properties.

**Acknowledgments** The authors warmly thank Luca Nodari (Institute of Condensed Matter Chemistry and Technology for Energy, ICMATE-CNR, Padova, Italy) for the Mössbauer experiments. The authors also gratefully acknowledge the French National Agency for Research (ANR, SmartCat Project, ref. ANR-18-CE07-0040-02), the Regional Council of Nouvelle Aquitaine, the French Ministry of Research and the European Regional Development Fund (ERDF) for financial supports.

## Reference

- [1] P. Whitaker *et al.*, *SAE Technical Paper* 2011-01-1219. DOI: 10.4271/2011-01-1219
- [2] Jiang D, Khivantsev K, Wang Y (2020) Low-Temperature Methane Oxidation for Efficient Emission Control in Natural Gas Vehicles: Pd and Beyond. *ACS Catal* 10:14304-14314 doi.org/10.1021/acscatal.0c03338
- [3] Gélin P, Primet M (2002) Complete oxidation of methane at low temperature over noble metal based catalysts: a review. *Appl. Catal., B*. 39:1–37.
- [4] Farrauto R. J. (2012) Low-temperature oxidation of methane. *Science* 337:659–660.
- [5] Raj A. (2016) Methane Emission Control. *Johnson Matthey Technol. Rev.*60(4):228–235
- [6] Richard M, Duprez D, Bion N, Can F (2016) Investigation of Methane Oxidation Reactions Over a Dual-Bed Catalyst System using  $^{18}\text{O}$  Labelled DRIFTS coupling. *ChemSusChem* 10(1):210-219 doi.org/10.1002/cssc.201601165.
- [7] Fujimoto K, Ribeiro F.H, Avalos-Borja M, Iglesia E (1998) Structure and Reactivity of  $\text{PdO}_x/\text{ZrO}_2$  Catalysts for Methane Oxidation at Low Temperatures. *J. Catal.* 179:431-442 doi.org/10.1006/jcat.1998.2178
- [8] Au-Yeung J, Chen K, Bell A.T, Iglesia E (1999) Isotopic Studies of Methane Oxidation Pathways on PdO Catalysts. *J. Catal.* 188:132-139 doi.org/10.1006/jcat.1999.2643
- [9] Cullis C.F, Willat B.M (1983) Oxidation of methane over supported precious metal catalysts. *J. Catal.* 83:267-285 doi.org/10.1016/0021-9517(83)90054-4
- [10] Chin Y.-H, Buda C, Neurock M, Iglesia E (2013) Consequences of metal–oxide interconversion for C–H bond activation during  $\text{CH}_4$  reactions on Pd catalysts. *J. Am. Chem. Soc.* 135:15425–15442
- [11] Richard M, Can F, Duprez D, Gil S, Giroir-Findler, Bion N (2014) Remarkable Enhancement of  $\text{O}_2$  Activation on Yttrium-Stabilized Zirconia Surface in a Dual Catalyst Bed. *Angewandte Chemie-International Edition* 53:11342-11345 DOI: 10.1002/anie.201403921
- [12] Richard M, Can F, Gil S, Giroir-Fendler A, Duprez D, Bion N (2016) Study of Lanthanum Manganate and Yttrium-Stabilized Zirconia-Supported Palladium Dual-Bed Catalyst System for the Total Oxidation of Methane: A Study by  $^{18}\text{O}_2/^{16}\text{O}_2$  Isotopic Exchange. *Chemcatchem* 8(11):1921-1928 doi.org.inc.bib.cnrs.fr/10.1002/cctc.201501398
- [13] Zhu J, Van Ommen J.G, Knoester A, Lefferts L (2005) Effect of surface composition of yttrium-stabilized zirconia on partial oxidation of methane to synthesis gas. *J. Catal.* 230:291-300 10.1016/j.jcat.2004.09.025
- [14] Répécaud PA, Kaper H, Richard M, Can F, Bion N (2017) Enhancement of Oxygen Activation and Mobility in  $\text{CaTi}_x\text{Fe}_{1-x}\text{O}_{3-\delta}$  Oxides. *ChemCat Chem* 9:2094-2098 10.1002/cctc.201700103
- [15] Pechini M.P, Method of Pre Parng Lead and Alkalne Earth Titanates and Nobates and Coat.,” US Pat. 3,330,697, p. 2, 1967
- [16] Danks A.E.,Hall S.R., Schnepf Z (2016) The evolution of ‘sol-gel’ chemistry as a technique for materials synthesis. *Mater. Horizons*, 3:91–112, doi: 10.1039/c5mh00260e
- [17] Rodriguez-Carvajal J (1990) FULLPROF: a program for Rietveld refinement and pattern matching.
- [18] Brunauer S, Emmett P.H (1937) The Use of Low Temperature van der Waals Adsorption Isotherms in Determining the Surface Areas of Various Adsorbents. *J. Am. Chem. Soc.*, 59(12):2682–2689 doi: 10.1021/ja01291a060.
- [19] Neimark A.V, Ravikovitch P.I, Grün M, Schüth F,Unger K.K (1998) Pore size analysis of MCM-41 type adsorbents by means of nitrogen and argon adsorption. *J. Colloid Interface Sci.*, 207(1):159–169 doi: 10.1006/jcis.1998.5748.
- [20] Drault F, Comminges C, Can F, Pirault-Roy L, Epron F, Le Valant A (2018) Palladium, iridium, and rhodium supported catalysts: Predictive  $\text{H}_2$  chemisorption by statistical cuboctahedron clusters model. *Materials (Basel)*. 11(5): 819 doi: 10.3390/ma11050819.
- [21] Martin D., Duprez D. (1996) Mobility of surface species on oxides. 1. Isotopic Exchange of  $^{18}\text{O}_2$  with  $^{16}\text{O}$  of  $\text{SiO}_2$ ,  $\text{Al}_2\text{O}_3$ ,  $\text{ZrO}_2$ ,  $\text{MgO}$ ,  $\text{CeO}_2$ , and  $\text{CeO}_2\text{-Al}_2\text{O}_3$ . Activation by noble metals. Correlation with oxide basicity. *J. Phys. Chem.* 1996, 100, 22, 9429–9438 ; doi.org/10.1021/jp9531568
- [22] Shannon R.D (1976) Revised Effective Ionic Radii and Systematic Studies of Interatomic Distances in Halides and Chalcogenides. *Acta Cryst* A32:751-767 doi: 10.1107/S0567739476001551
- [23] Lin S, Yang L, Yang X, Zhou R (2014) Redox properties and metal–support interaction of  $\text{Pd/Ce}_{0.67}\text{Zr}_{0.33}\text{O}_2\text{-Al}_2\text{O}_3$  catalyst for CO, HC and  $\text{NO}_x$  elimination. *Appl. Surf. Sc.* 305: 642-649 doi.org/10.1016/j.apsusc.2014.03.153
- [24] Duprez D (2006) *Isotopes in Catalysis*. Catalytic Science Series 4, Imperial College Press, London, 133 –181
- [25] Mahara Y, Murata K, Ueda K, Ohyama J, Kato K, Satsuma A (2018) Time Resolved in situ DXAFS Revealing Highly Active Species of PdO Nanoparticle Catalyst for  $\text{CH}_4$  Oxidation. *ChemCatChem* 10(16): 3384–3387 doi: 10.1002/cctc.201800573.
- [26] Farrauto R.J, Lampert J.K, Hobson M.C, Waterman E.M (1995) Thermal decomposition and reformation of PdO catalysts; support effects. *Appl. Catal. B, Environ.*, 6(3): 263–270 doi: 10.1016/0926-3373(95)00015-1.
- [27] Su S.C, Carstens J.N, Bell A.T (1998) A study of the dynamics of Pd oxidation and PdO reduction by  $\text{H}_2$  and  $\text{CH}_4$ . *J. Catal.*, 176: 125–135 doi: 10.1006/jcat.1998.2028.

- 
- [28] Seiyama T (1992) Total Oxidation of hydrocarbons on perovskite oxides. *Catal. Rev.* 34(4): 281-300 doi: 10.1080/01614949208016313.
- [29] Sun L, Wang Y, Guan N, Li L (2020) Methane Activation and Utilization: Current Status and Future Challenges. *Energy Technol.*, 8(8): 1-13 doi: 10.1002/ente.201900826.
- [30] Burch R, Urbano F.J (1995) Investigation of the active state of supported palladium catalysts in the combustion of methane. *Appl. Catal. A: Gen.* 124(1):121-138 doi.org/10.1016/0926-860X(94)00252-5
- [31] Burch R, Crittle D.J, Hayes M.J (1999) C–H bond activation in hydrocarbon oxidation on heterogeneous catalysts. *Catal. Today* 47:229-234 doi.org/10.1016/S0920-5861(98)00303-4
- [32] Burch R, Urbano F.J, Loader P.K (1995) Methane combustion over palladium catalysts: The effect of carbon dioxide and water on activity. *Appl. Catal. A: Gen.* 123:173-184 doi: 10.1016/0926-860X(94)00251-7
- [33] Ciuparu D, Perkins E, Pfefferle L (2004) In situ DR-FTIR investigation of surface hydroxyls on  $\gamma$ -Al<sub>2</sub>O<sub>3</sub> supported PdO catalysts during methane combustion. *Appl. Catal. A: Gen.* 263:145-153 DOI:10.1016/j.apcata.2003.12.006.
- [34] Ojala S, Bion N, Rijo Gomes S, Keiski R.L, Duprez D (2010) Isotopic oxygen exchange over Pd/Al<sub>2</sub>O<sub>3</sub> Catalyst: Study on C<sup>18</sup>O<sub>2</sub> and <sup>18</sup>O<sub>2</sub> exchange. *ChemCatChem* 2:527–533 doi: 10.1002/cctc.201000033.
- [35] Schwartz W.R., Pfefferle L.D. (2012) Combustion of Methane over Palladium-Based Catalysts: Support Interactions. *J. Phys. Chem. C.* 116: 8571-8578 doi.org/10.1021/jp2119668
- [36] Khan H.A, Hao J, El Tall O, Farroq A. (2021) Yttrium stabilization and Pt addition to Pd/ZrO<sub>2</sub>catalyst for the oxidation of methane in the presence of ethylene and water. *RSC Adv.* 11(20) 11910–11917 doi: 10.1039/d0ra10773e